de Matos Simoes et al., http://www.jcb.org/cgi/content/full/jcb.201307070/DC1

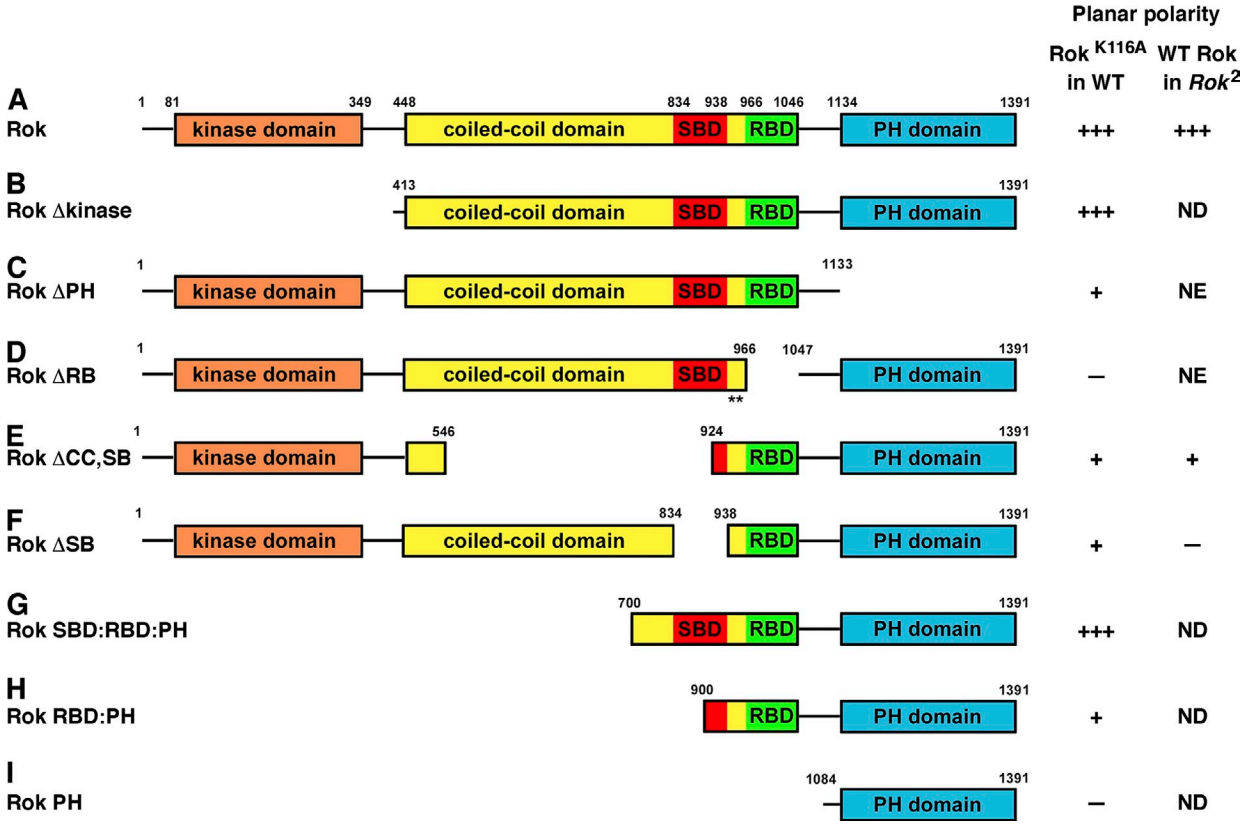

Figure S1. **Rho-kinase transgenes for structure/function analysis.** Schematic of Rho-kinase deletion transgenes. (A) Full-length Rho-kinase (Rok, aa 1–1,391). N-terminal serine/threonine kinase domain (aa 81–349), central coiled-coil domain (CC, aa 448–1,046), Shroom-binding domain (SB, aa 834–938), Rho GTPase-binding domain (RB, aa 966–1,046), and C-terminal pleckstrin homology domain (PH, aa 1,134–1,391) are shown. (B) Rok Δkinase (aa 413–1,391). (C) Rok ΔPH (aa 1–1,133). (D) Rok ΔRB (Δaa 967–1,046) and K948M, L955A. (E) Rok ΔCC,SB (Δaa 547–923). (F) Rok ΔSB (Δaa 835–937). (G) Rok SB:RB:PH (aa 700–1,391). (H) Rok RB:PH (aa 900–1,391). (I) Rok PH (aa 1,084–1,391). Transgenes were N-terminal Venus fusions inserted in the attP40 site on chromosome II, except for Rok PH (an N-terminal HA fusion analyzed by mRNA injection). (left column) Inactive Rok^{K116A} proteins were expressed in wild-type embryos. (right column) Active, wild-type Rok proteins were expressed in *Rok*^{2} maternal mutants. The extent of planar polarity is indicated (+++, wild-type planar polarity; +, intermediate; –, no planar polarity; NE, no embryos at the correct stages as a result of earlier defects; ND, not done). WT, wild type. See Fig. 1 and Fig. S2 for images and quantification.

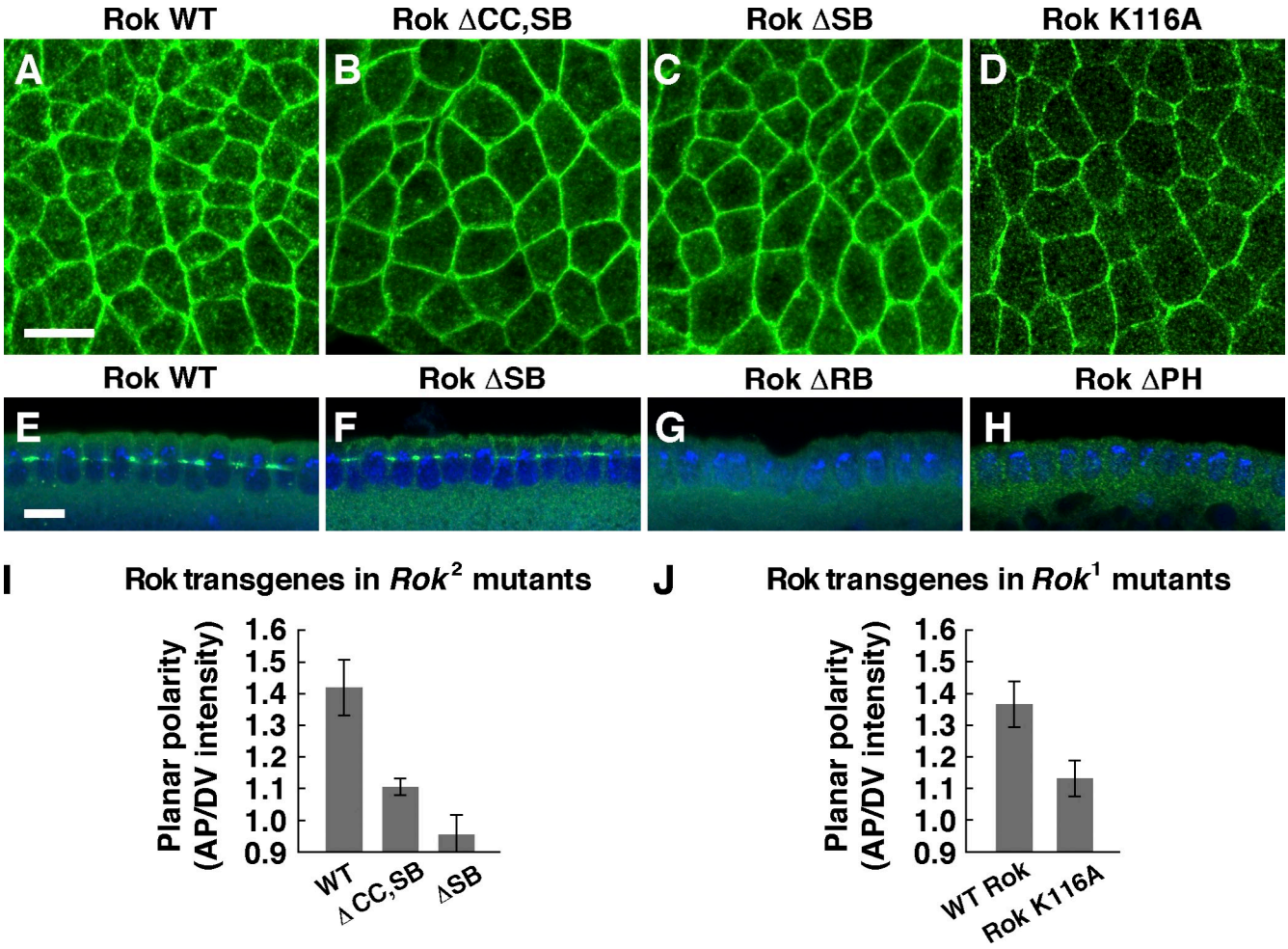

Figure S2. **Expression of Rho-kinase transgenes in *Rho-kinase* mutants.** (A–H) Localization of wild-type Venus:Rok proteins in stage 7 *Rok* mutants expressing wild-type Rok (WT; A and E), Rok ΔCC,SB (B), Rok ΔSB (C and F), Rok^{K116A} (D), Rok ΔRB (G), and Rok ΔPH (H) in Rok^{2} maternal mutants (Rok^{1} in D). Rok transgenes (anti-GFP, green) and nuclei (DAPI, blue) are shown. Rok ΔRB and Rok ΔPH fail to localize to the cellularization front in Rok^{2} mutants, and these embryos arrest in midcellularization, possibly because of deregulated Rok activity. (A–D) Anterior is left, and ventral is down. (E–H) Cross sections, with apical up. (I and J) Planar polarized enrichment of Rok proteins at AP cell boundaries (75–90° with respect to the AP axis) relative to DV cell boundaries (0–15°) in Rok^{2} (I) and Rok^{1} (J) maternal mutants. Rok ΔCC,SB, Rok ΔSB, and Rok^{K116A} were significantly less planar polarized than wild-type Rok when expressed in *Rok* mutants ($P \leq 0.04$). A single value was obtained for each image by averaging 100–200 edges per image; 4–9 images in 4–9 embryos were analyzed/genotype. Means ± SEM between images are shown. Bars, 10 µm.

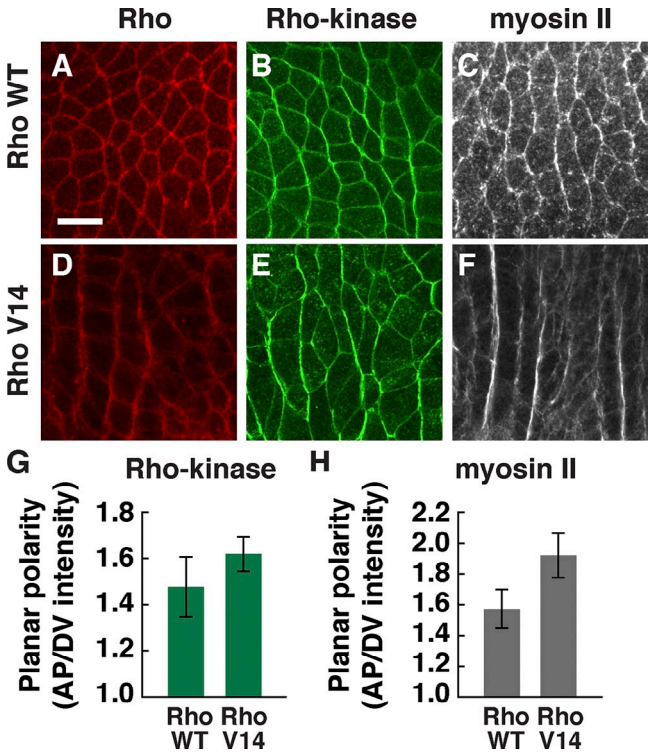

Figure S3. **Activated Rho^{V14} promotes Rho-kinase and myosin II planar polarity at the lateral cell membrane.** (A–F) Localization of HA:Rho (red), Venus:Rho-kinase^{K116A} (green), and Myo:GFP (white) in stage 7 embryos expressing wild-type (WT) HA:Rho (A–C) or constitutively active HA:Rho^{V14} (D–F; D and F show more lateral planes). Note that Rho^{V14} displays a localized enrichment at a subset of AP edges at the lateral cell membrane. Anterior is left, and ventral is down. (G and H) Planar polarized enrichment of Venus:Rho-kinase (G) and Myo:GFP (H) at AP cell boundaries (75–90° with respect to the AP axis) relative to DV cell boundaries (0–15°) in Rho^{WT}- and Rho^{V14}-injected embryos. Rho^{V14} locally increased Rho-kinase and myosin accumulation in basal planes but did not significantly alter the degree of overall Rho-kinase planar polarity ($P = 0.41$) or myosin planar polarity ($P = 0.11$) compared with embryos expressing Rho^{WT}. A single value was obtained for each image by averaging 100–200 edges per image; 6–17 images in 3–12 embryos were analyzed/genotype. Means ± SEM between images are shown. Bar, 10 µm.

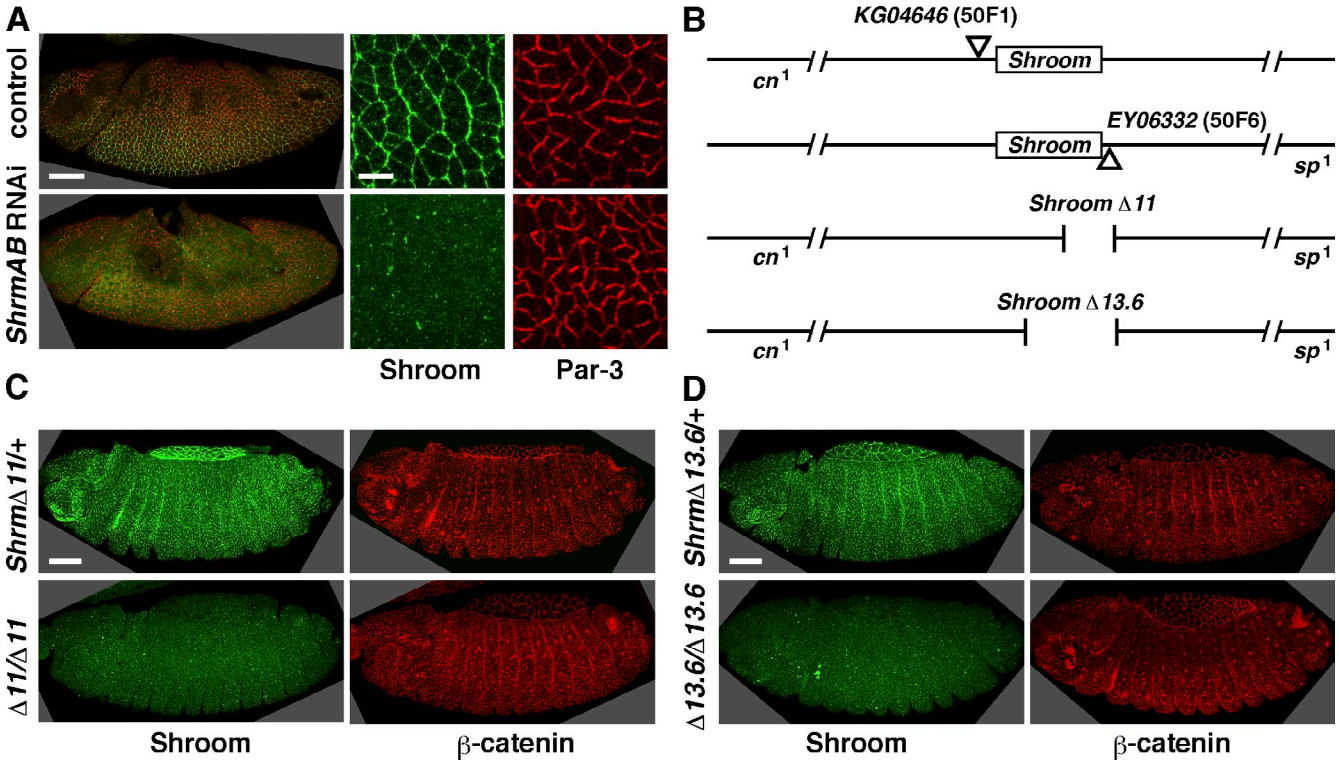

Figure S4. **Shroom junctional levels are strongly reduced in *Shroom* mutant and *Shroom* RNAi embryos.** (A) Localization of Shroom (green) and Baz/Par-3 (red) in control water-injected (top) and *ShrmAB* RNAi embryos overexpressing Dicer-2 (bottom) at stage 8. (B) Generation of $Shrm^{\Delta 11}$ and $Shrm^{\Delta 13.6}$ deletions lacking part of the *Shroom* coding sequence by male-specific *P* element–mediated recombination. The proximal [P(SUPor-P)KG04646 at 50F1] and distal [$P(EPgy2)CG8613^{EY06332}$ at 50F6] *P* elements were combined in trans and simultaneously excised by transposase expression. Deletions removing parts of the intervening Shroom coding sequence were identified by the presence of cn^1 and sp^1 recombined in cis with the proximal and distal *P* elements, respectively. The $Shrm^{\Delta 11}$ and $Shrm^{\Delta 13.6}$ deletion breakpoints were molecularly mapped by PCR (see Materials and methods). The 5′ breakpoint of $Shrm^{\Delta 11}$ is between 10,217,297 and 10,238,252, and the 3′ breakpoint is between 10,238,326 and 10,239,796 on chromosome 2R. The 5′ breakpoint of $Shrm^{\Delta 13.6}$ is between 10,215,313 and 10,217,297, and the 3′ breakpoint is between 10,238,326 and 10,239,743. Both deletions retain sequences immediately outside of the two *P* elements as well as sequences in the 5′ coding region, likely because of gap repair. Both deletions remove sequences within the last three exons of Shroom, which encode the Rho-kinase–binding domain. In addition, $Shrm^{\Delta 13.6}$ (but not $Shrm^{\Delta 11}$) removes sequences within the centrally located exons 6 and 7. (C and D) Heterozygous (top) and homozygous *Shroom* mutant (bottom) embryos stained with antibodies to Shroom (green) and β-catenin (red). Shroom protein was not detected in embryos homozygous for $Shrm^{\Delta 11}$ (C) or $Shrm^{\Delta 13.6}$ (D). Homozygous mutant embryos were identified by the absence of GFP from a CyO, twist-Gal4, UAS-GFP balancer and hand selected before fixation. Anterior is left, and ventral is down. Bars, 10 µm.

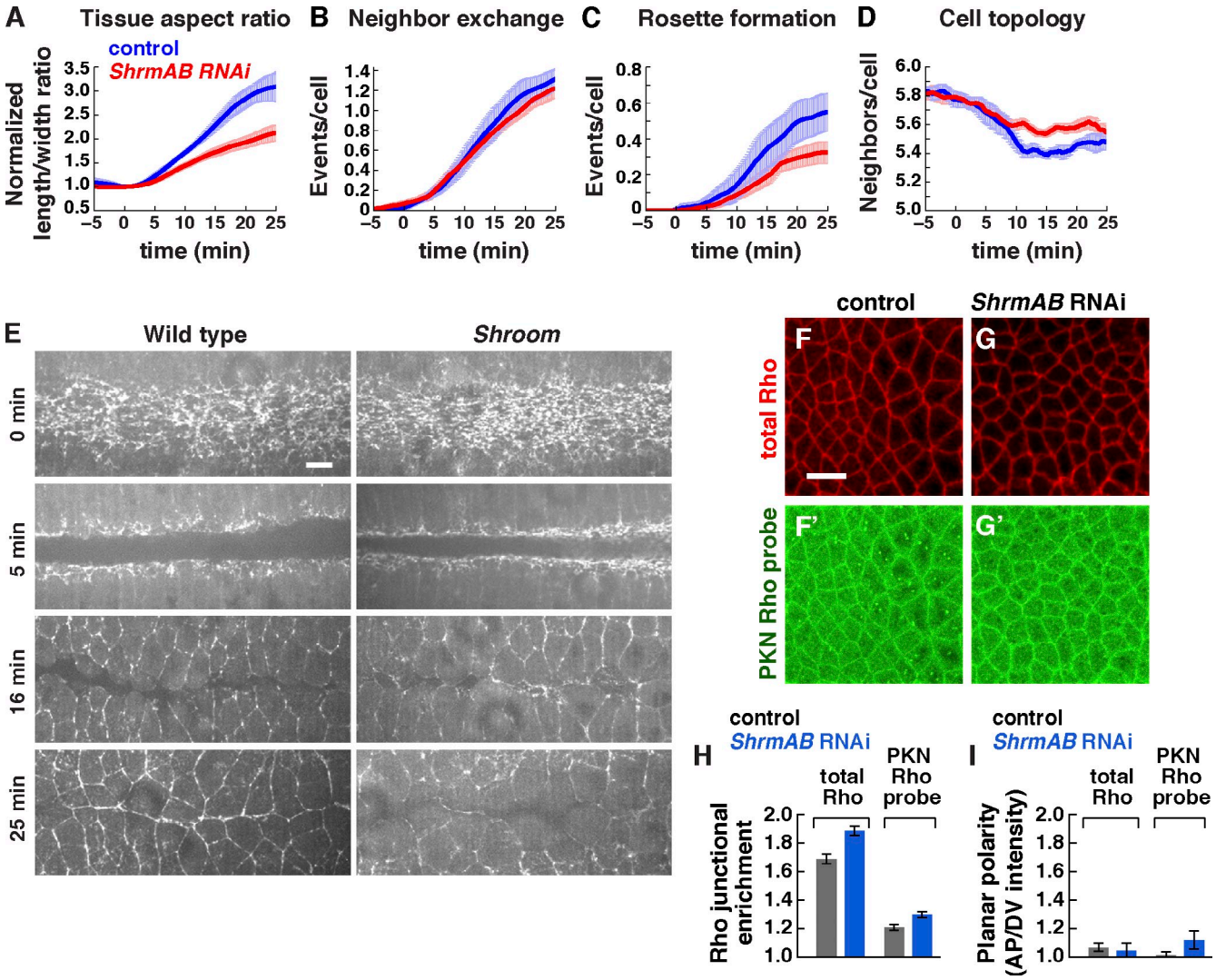

Figure S5. **Cell behavior and Rho GTPase signaling in *Shroom* mutant and *Shroom* RNAi embryos.** (A–D) Cell behavior in control *flp* RNAi (blue) and *ShrmAB* RNAi (red) embryos (t = 0 is the onset of elongation in early stage 7). (A) Tissue aspect ratio (tissue length along the AP axis relative to its width along the DV axis) normalized to the value at t = 0. *ShrmAB* RNAi embryos have a reduced tissue aspect ratio in stage 8 compared with control embryos (P = 0.01 at 15 min, P = 0.007 at 20 min, and P = 0.04 at 30 min). (B and C) Neighbors lost per cell through local neighbor exchange, also known as a T1 process (resulting from single edge contraction events; B) and rosette formation (resulting from the contraction of multiple, consecutive edges; C). Rosette formation was reduced in *ShrmAB* RNAi embryos (P = 0.08 at 30 min) but did not reach statistical significance, likely as a result of the partial effects of RNA knockdown. Local neighbor exchange was not significantly affected (P = 0.49 at 30 min). (D) Mean number of neighbors per cell. Cells in control *flp* RNAi embryos have progressively fewer neighbors midway through elongation as a result of cell rearrangement. *ShrmAB* RNAi embryos have more neighbors on average midway through elongation (P = 0.018 at 20 min), consistent with reduced cell rearrangement. Videos of three control *flp* RNAi and four *ShrmAB* RNAi embryos were analyzed at 15-s intervals (177–266 cells tracked/embryo). Means ± SEM between embryos are shown. (E) Stills of time-lapse videos showing ventral furrow formation in wild-type (left) and $Shrm^{\Delta 11}$ mutant (right) embryos expressing Myo:GFP. Apical myosin accumulation occurs normally in *Shroom* mutants (0 min), and furrow invagination (5 min) and closure (16 min) progress with the same timing as in wild type (8/8 videos of $Shrm^{\Delta 11}$ mutant embryos). Ventral views, with anterior left. (F and G) Total Rho protein (anti-Rho) and PKNG58A:Venus (PKN Rho probe) in water-injected (F) and *ShrmAB* RNAi (G) embryos. Anterior is left, and ventral is down. (H) Junctional enrichment of total Rho protein and PKN Rho probe signal relative to the medial cell cortex. (I) Planar polarized enrichment of total Rho protein and the Rho probe at AP cell boundaries (75–90° with respect to the AP axis) relative to DV cell boundaries (0–15°) was not significantly different between *ShrmAB* RNAi embryos and water-injected controls. A single value was obtained for each image by averaging 100–200 edges/image; 4–12 images in 4–12 embryos were analyzed/genotype. Means ± SEM between images are shown. Bars: (E) 5 µm; (F and G) 10 µm.

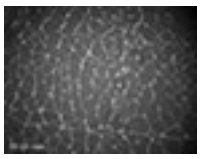

Video 1. **Myosin II junctional and medial populations in a wild-type embryo.** A wild-type embryo expressing Myo:GFP. Note two populations of myosin II, one associated with adherens junctions at AP cell boundaries and a highly dynamic pool at the medial–apical cell cortex. Images were acquired with a spinning-disk confocal microscope (UltraView RS5; PerkinElmer) at 63× magnification, with 5-s intervals in early stage 8. Anterior is left, and ventral is down.

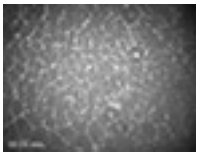

Video 2. **Myosin II junctional and medial populations in a *Shroom* mutant embryo.** *Shrm*$^{\Delta 11}$ mutant embryo expressing Myo:GFP. The junctional pool of myosin II at AP boundaries is strongly reduced compared with wild type. Images were acquired with a spinning-disk confocal microscope (UltraView RS5; PerkinElmer) at 63× magnification, with 5-s intervals in early stage 8. Anterior is left, and ventral is down.

Video 3. **Myosin II dynamics in a wild-type embryo.** Wild-type embryo expressing Myo:GFP. Myosin II is enriched at AP cell boundaries during axis elongation. Images were acquired with a spinning-disk confocal microscope (UltraView RS5; PerkinElmer) at 40× magnification, with 30-s intervals in stages 7–8. Anterior is left, and ventral is down.

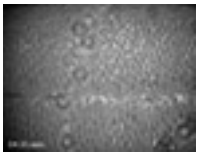

Video 4. **Myosin II dynamics in a *Shroom* mutant embryo.** *Shrm*$^{\Delta 11}$ mutant embryo expressing Myo:GFP. Myosin II cortical localization is not maintained at AP cell boundaries during elongation. Images were acquired with a spinning-disk confocal microscope (UltraView RS5; PerkinElmer) at 40× magnification, with 30-s intervals in stages 7–8. Anterior is left, and ventral is down.

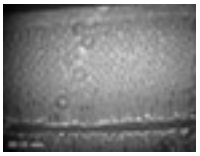

Video 5. **Myosin II dynamics in a control injected embryo.** Wild-type *flp* RNAi embryo expressing Myo:GFP and overexpressing Dicer-2. Myosin II is enriched at AP cell boundaries during axis elongation. Images were acquired with a spinning-disk confocal microscope (UltraView RS5; PerkinElmer) at 40× magnification, with 30-s intervals in stages 7–8. Anterior is left, and ventral is down.

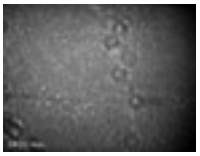

Video 6. **Myosin II dynamics in a *ShrmA* RNAi embryo.** *ShrmA* RNAi embryo expressing Myo:GFP and overexpressing Dicer-2. Myosin II cortical localization is not maintained at AP cell boundaries during elongation. Images were acquired with a spinning-disk confocal microscope (UltraView RS5; PerkinElmer) at 40× magnification, with 30-s intervals in stages 7–8. Anterior is left, and ventral is down.

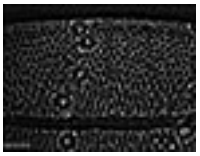

Video 7. **Cell behavior in a wild-type embryo.** Wild-type embryo expressing Spider:GFP. Images were acquired with a spinning-disk confocal microscope (UltraView RS5; PerkinElmer) at 40× magnification, with 15-s intervals in stages 6–8. Anterior is left, and ventral is down.

Video 8. **Cell behavior in a *Shroom* mutant embryo.** *Shrm*$^{\Delta 11}$ mutant embryo expressing Spider:GFP. Images were acquired with a spinning-disk confocal microscope (UltraView RS5; PerkinElmer) at 40× magnification, with 15-s intervals in stages 6–8. Anterior is left, and ventral is down.